Advances in Water Resources 178 (2023) 104493

Contents lists available at ScienceDirect

Advances in Water Resources

journal homepage: www.elsevier.com/locate/advwatres

Geomorphic floodplain mapping in small Mediterranean catchments using LiDAR data

Claudia Deiana [a], Roberto Deidda [a], Francesco Viola [a,*]

[a] Università degli Studi di Cagliari, Cagliari, CA, Italy

ARTICLE INFO

Keywords:
Floodplain mapping
Flood descriptors
Scaling laws
Digital elevation model

ABSTRACT

Recent advances in remote sensing technologies along with the increased availability of topographic data have lately encouraged the development of automatic DEM (Digital Elevation Model)-based procedures for floodplain delineation. Geomorphic methods, establishing relationships between flood descriptors and morphologic catchment characteristics, appear particularly suitable to be implemented within a GIS algorithm. In the present work, four simplified geomorphic approaches based on "flow-depth scaling laws" (FD) or "flow-cross-sectional area scaling laws" (FA) with contributing area and two methods employing two different flood descriptors (Hydro-Geomorphic Method, HGM and Geomorphic Flood Index method, GFIM) have been applied for the preliminary evaluation of floodplain extent using high resolution DEMs (i.e. LiDAR at 1 and 2 m resolution) as the main input. Taking as a case study six of the largest basins located in southern Italy, the performances of these methods were evaluated and critically compared using government agency derived flood hazard maps as benchmarks. Results show that the adoption of FD especially when combined with morphology to formulate the GFIM, allows to efficiently predict the flood-prone areas with low computational costs. At the same time, performances of the flood mapping procedures based on "flow-area scaling laws", although in principle more appealing, seem to be slightly lower. Overall, the proposed approaches can be applied for rough mapping of floodplains in ungauged basins or in data-scarce regions where standard flood hazard maps are unavailable.

1. Introduction

Identification of flood-prone areas has become an urgent challenge in flood risk management, representing a key task to reduce flood damages and minimise loss of life during extreme events. According to the Emergency Events Database (EM-DAT) maintained by the Centre for Research on the Epidemiology of Disasters (CRED), in the 20-year period between 2000 and 2019 floods have been the most frequently occurring type of natural disaster, accounting for 44% of total events, affecting 1.6 billion people worldwide and leading to approximately US$ 651 billion in economic losses (CRED, 2020). Furthermore, floods intensity and frequency are expected to increase due to climate change over the next decades. Scientific evidence indicates that these trends are partially attributable to the global temperature rise, which according to Clausius-Clapeyron relation leads to a greater moisture-holding capacity of the atmosphere, thus resulting in an increase of rainfall extremes (Fowler et al., 2021). The severe flooding observed in Western Germany during July 2021 (Lehmkuhl et al., 2022) which caused nearly 200 fatalities, suggests that climate disruption is already revealing its impact on weather patterns, making the implementation of effective flood risk mitigation strategies one of the most pressing needs of our time.

Flood inundation maps represent useful tools helping urban planners and stakeholders to identify which areas could potentially be affected by these natural phenomena. Their effectiveness has been widely recognised to the point that among EU (European Union) member states it has become mandatory to map flood extent since Directive 2007/60/EC has entered into force, while in the United States such maps are provided by the Federal Emergency Management Agency (FEMA) to support the National Flood Insurance Program. Traditional floodplain mapping techniques entail significant data collection as they usually involve both hydrologic and hydraulic analyses. When the stream gauge network is sparse and historical rainfall series are the only type of accessible data over a given region, hydrological modelling allows the assessment of hydrographs associated with specific return periods. Rainfall-runoff models would normally receive as the main input a hyetograph based on the intensity-duration-frequency curve (IDF curve) valid for the study area. IDF curves are typically obtained through complex procedures involving statistical analysis of long-term historical rainfall observations

* Corresponding author.
E-mail address: viola@unica.it (F. Viola).

https://doi.org/10.1016/j.advwatres.2023.104493
Received 6 March 2023; Received in revised form 29 May 2023; Accepted 16 June 2023
Available online 17 June 2023

(Deidda et al., 2021); their update under the conditions of a changing climate is a modern challenge (Forestieri et al., 2018). By simulating the physical processes involved in the transformation of rainfall into runoff, hydrological models provide as output hydrographs of assigned return period, which are then used as input of hydraulic models to simulate the flood propagation over complex domains. Their setup requires accurate topographic information on river features and artificial structures along the reach (e.g. bridges, culverts, levees), evaluation of surface roughness and the assignment of appropriate boundary conditions. Hydraulic simulations are also time-consuming and computationally intensive, other than being costly. All in all, conventional floodplain mapping approaches are difficult to apply, especially in those regions where hydrological and morphological data are scarce.

In recent years, the increasing availability of high resolution DEMs has encouraged the development of alternative cost-effective procedures based on river basin geomorphic features to perform preliminary floodplain delineation in ungauged areas. These methods rely on the assumption that floodplains are the end-product of the accumulated effects of flood events occurred over time and are therefore characterized by unique geomorphic and hydrologic properties that make them distinguishable from adjacent hillslopes (Nardi et al., 2006). Various authors successfully experimented hydrogeomorphic approaches based on the application of hydraulic geometry relations (Leopold and Maddock, 1953; Bhowmik, 1984), highlighting their potential capabilities in flood-prone areas detection. The term 'hydraulic geometry' was first introduced by Leopold and Maddock (1953) to describe those relationships between stream channel hydraulic characteristics and discharge at any river cross section. Subsequently, Bhowmik (1984) supposed that the concept of hydraulic geometry could also be applied to define floodplains characteristics and proved the existence of simple scaling laws relating floodplains hydraulic properties (e.g. width, flow area, flow depth) to the upstream contributing area. Such relationships have received increasing attention in recent investigations as they allow to easily estimate hydraulic status that, conversely, would normally be evaluated through hydraulic simulations and, moreover, they appear particularly suitable to be implemented within GIS-based procedures.

For example, Nardi et al. (2006, 2013, 2019) proposed an algorithm that identifies floodplain extent by comparing river corridors terrain elevation with the absolute elevation of a variable flow depth, estimated as a function of contributing area at each stream cell through a stream-order averaged scaling law. The scaling parameters were initially estimated using water depth values derived from Manning equation in conjunction with GIUH (Geomorphologic Instantaneous Unit Hydrograph) peak discharge (Rodríguez-Iturbe et al., 1979; Rodriguez-Iturbe, 1993), while, in a global scale application, Nardi et al. (2019) proved that optimal parameterization obtained through a simple calibration performed with reference maps provides consistent results, while being less computational demanding. In a recent study, Annis et al. (2022) investigated the influence of morphologic and climatic river basin characteristics on the parameters of the scaling law between flow depth and drainage area, demonstrating that enhanced performances can be achieved considering parameterization for different ranges of slopes and average annual rainfall. Other researchers implemented linear binary classification procedures and assessed the performance of several classifiers in identifying areas exposed to flood hazard. For example, Degiorgis et al. (2012) applied a threshold binary classification technique employing different classifiers derived from single DEM-based morphological features. This approach has been reapplied by Manfreda et al. (2014) to carry out a comparative analysis with the hydrogeomorphic algorithm (Nardi et al., 2006) and the modified Topographic Index method (Manfreda et al., 2011). In another work, Samela et al. (2017) compared the performance of eleven classifiers applied at continental scale and investigated the transferability of the corresponding optimal thresholds with varying topography and calibration area extent. According to the authors, a calibration area at least equal to 2% of the total drainage area of interest allows to determine a threshold value close enough to the optimal one. Their results also showed that amongst all the tested flood descriptors, the Geomorphic Flood Index (GFI) appeared more transferrable than others in areas with varying topography, providing the most reliable and accurate floodplain delineation.

The aforementioned studies have been carried out utilizing DEMs with grid resolution ranging from 30-m to 250-m which allow to rapidly produce inundation maps at large scale. In a different effort, Zheng et al. (2018) presented a new effective workflow combining the HAND (Height Above Nearest Drainage) method (Rennó et al., 2008; Nobre et al., 2016) with an automatic channel network extraction procedure (Passalacqua et al., 2010) that avails of high resolution topographic data (e.g. 3-m resolution DEM) without compromising computational efficiency. To date, similar applications of hydrogeomorphic methodologies employing information obtained from DEMs at very high resolution are still exiguous.

The present work aims to investigate the performance of four geomorphic approaches at the basin scale coupling estimations from two simple power laws relating upstream contributing area to cross-sectional flow depth and flow area (hereafter referred to as "flow-depth scaling laws" (FD) and "flow-area scaling laws" (FA), respectively), and two mapping methods named Hydro-Geomorphic Method (HGM) and Geomorphic Flood Index Method (GFIM). The flood-prone areas in HGM methods are identified by comparing a variable flow depth computed along the reach to the relative elevation of those cells hydrologically connected to the stream, following the algorithm described by Nardi et al. (2019). Instead, the GFIM methods avail of the Geomorphic Flood Index (Samela et al., 2017) as a flood descriptor and utilize the threshold binary classification to discern between flooded or not flooded areas. The HGM-FD and the GFIM-FD methods take advantage of the straightforward relation between the flow depth and the drainage area (flow-depth scaling laws, FD), whilst the HGM-FA and the GFIM-FA make use of the scaling law relating cross-sectional flow area to contributing area (flow-area scaling laws, FA).

While the implementation of floodplain mapping procedures taking advantage of the scaling relation between flow depth and contributing area (flow-depth scaling laws, FD) has already been experimented in other studies, to our best knowledge, flow-area scaling laws (FA), relating cross-sectional flow area to drainage area, represent an element of novelty of this work that in our opinion deserve to be investigated. Indeed, we should expect, in principle, a stronger dependence of the flow area, rather than the flow depth, on the contributing area since the flow depth is more affected by the river cross-section shape, as will be discussed in the Appendix. It is worth noticing that the application of HGM-FA and the GFIM-FA methods requires the identification of a flow depth-flow area relationship (FDFA) in each river cross-section considered in the analysis, or alternatively implies some additional steps which can be synthesized in the implementation of a root-finding algorithm that allows to approximately estimate the flow depth associated with a flow area value in any given river cross-section of known profile.

The considered floodplain mapping procedures were implemented in a GIS environment using as primary input the information extracted from high resolution DEMs derived from LiDAR surveys at 1-m and 2-m resolution in Sardinia and Sicily (Italy), respectively. Official flood hazard maps, provided by regional Agiencies, were used to calibrate the four approaches and then as a benchmark to evaluate the performances on three major river basins in Sicily and three major rivers in Sardinia, applying standard indices based on contingency tables and commonly employed for forecast verification.

This paper is organised as follows: Section 2 describes the methodology and the implementation of the four approaches, with details on flood descriptors and the geomorphic power laws. The study area and dataset, including terrain data and official flood hazard maps, are presented in Section 3. In Section 4, outcomes form the application of the four approaches are illustrated and then discussed in Section 5 along with their strengths and limitations. Finally, Section 6 summarizes the

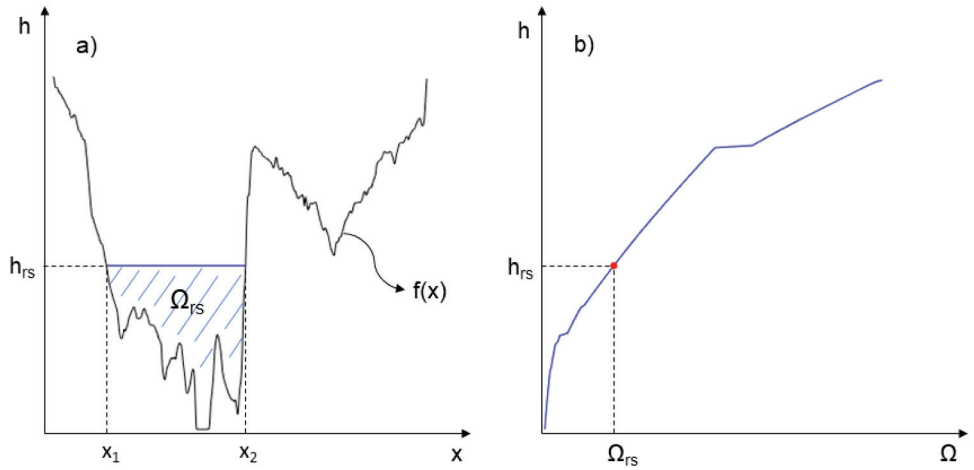

Fig. 1. (a) Example of floodplain cross-section shape f(x) and (b) corresponding flow depth-flow area relationship (FDFA), see eq. (3).

main results and suggestions for further studies. A Flowchart of the four implemented methods used to obtain floodplain mapping based on FD or FA is reported in the supplementary material (Figure S1).

2. Methodology

2.1. Flood descriptors and geomorphic scaling laws

In this section, the main assumptions of the four considered geomorphic approaches to map expected flood-prone areas in the river basins of interest are introduced and described. The core of all the methods relies on the definition of flood descriptors based on an empirically estimated water level. Flood descriptors can be considered as potential indicators of the susceptibility of an area to be flooded: starting from the topographic data contained in DEMs, they can be calculated through proper procedures and then represented in a gridded layer.

The four considered approaches require a preliminary terrain analysis to assign to each grid cell (i,j) of the DEM a flow direction D_{ij} and a corresponding flow accumulation F_{ij}, and subsequently to obtain the river network binary raster. In this work, these operations were performed with the r.watershed module of the GRASS GIS (Jasiewicz and Metz, 2011), using the D8 single-direction flow algorithm (O'Callaghan and Mark, 1984). Stream network is identified by flagging cells (r,s) with a flow accumulation F_{rs} exceeding a constant predefined threshold. Also, the drainage area A_{rs} at any stream cell (r,s) can be immediately calculated as the product between the local flow accumulation F_{rs} and the cell size.

Once flow accumulation F_{rs} and the drainage area A_{rs} layers are extracted from the DEM as described above, we assign to each river network cell (r,s) a variable flood stage h_{rs} above the thalweg derived through simple geomorphic scaling laws, as defined below. The HGM-FD and the GFIM-FD methods make use of a relation that expresses the flow depth above riverbed h_{rs}^{FD} as a function of the contributing area A_{rs} (the apex FD indicates the flow-depth scaling law), as suggested by Leopold and Maddock (1953):

$$h_{rs}^{FD} = a(A_{rs})^b \tag{1}$$

while the HGM-FA and GFIM-FA methods make use of a relation that expresses the cross-sectional flow area Ω_{rs} as a function of the contributing area A_{rs} (flow-area scaling laws, FA), as suggested by Leopold and Maddock (1953):

$$\Omega_{rs} = c(A_{rs})^d \tag{2}$$

consequently, the flow depth above riverbed h_{rs}^{FA} is indirectly estimated by a flow depth-flow area relationship (FDFA):

$$h_{rs}^{FA} = FDFA(\Omega_{rs}) \tag{3}$$

Calibration of parameters *a, b, c,* and *d* of the scaling laws in Eqs. (1) and (2) is described later in Section 2.2. Afterwards, availing of the information contained in the flow direction layer, we assign to each grid cell (i,j) the flow depth above riverbed h_{rs} obtained by Eq. (1) or Eq. (3) in the nearest stream cell (r,s) hydrologically connected to (i,j):

$$h_{ij}^{FD} = h_{rs}^{FD} \tag{4}$$

$$h_{ij}^{FA} = h_{rs}^{FA} \tag{5}$$

Eqs. (1) and (2) are based on the hydraulic geometry concepts developed by Leopold and Maddock (1953) as they allow to approximately determine stream channel characteristics as functions of a morphological feature, namely the upslope contributing area. While the main advantage of these scaling laws relies in their straightforward implementation in DEM-based routines, it is important to underline that these relations are not able to describe hydraulic processes as traditional modelling techniques do, such as the effects induced by the presence of artificial infrastructures along the stream, sudden changes in channel geometry, riverbed slope or roughness. However, despite its simplicity, flow-depth scaling law (FD) in Eq. (1), relating flow depth and contributing area, has been proven promising and partially able to reproduce some physical phenomena (Manfreda et al., 2014; Samela et al., 2017; Nardi et al., 2019; Tavares da Costa et al., 2020). In addition, as discussed in the Introduction, we were motivated to also investigate the feasibility and performances of methods based on flow-area scaling laws (FA), relating cross-sectional flow area and contributing area. Indeed, while the behaviour of the flow depth is subject to great uncertainty when moving from upstream to downstream along the same river (especially when the bank-full stage is exceeded or in highly irregular cross-sections), the flow area is expected to regularly increase as the drainage area increases, so in principle one should prefer FA approaches. Such behaviour was also confirmed through numerical simulations of flow propagation on synthetical catchments with constant and varying cross-sections along the river (see Appendix for details), supporting the expected advantages of flow-area scaling laws (FA) as opposed to flow-depth scaling laws (FD).

As a practical way to the estimation of the flow depth-flow area (FDFA) relationship between h_{rs} and Ω_{rs} in Eq. (3), an automatic procedure based on the bisection method was also developed. Namely, this procedure is aimed to calculate a flow depth h_{rs} associated with the flow area Ω_{rs} obtained through Eq. (2). In any specific river cross-section of interest, given a cross-section profile, a flow depth h_{rs} is iteratively assigned until its corresponding flow area value (i.e. the cross-section

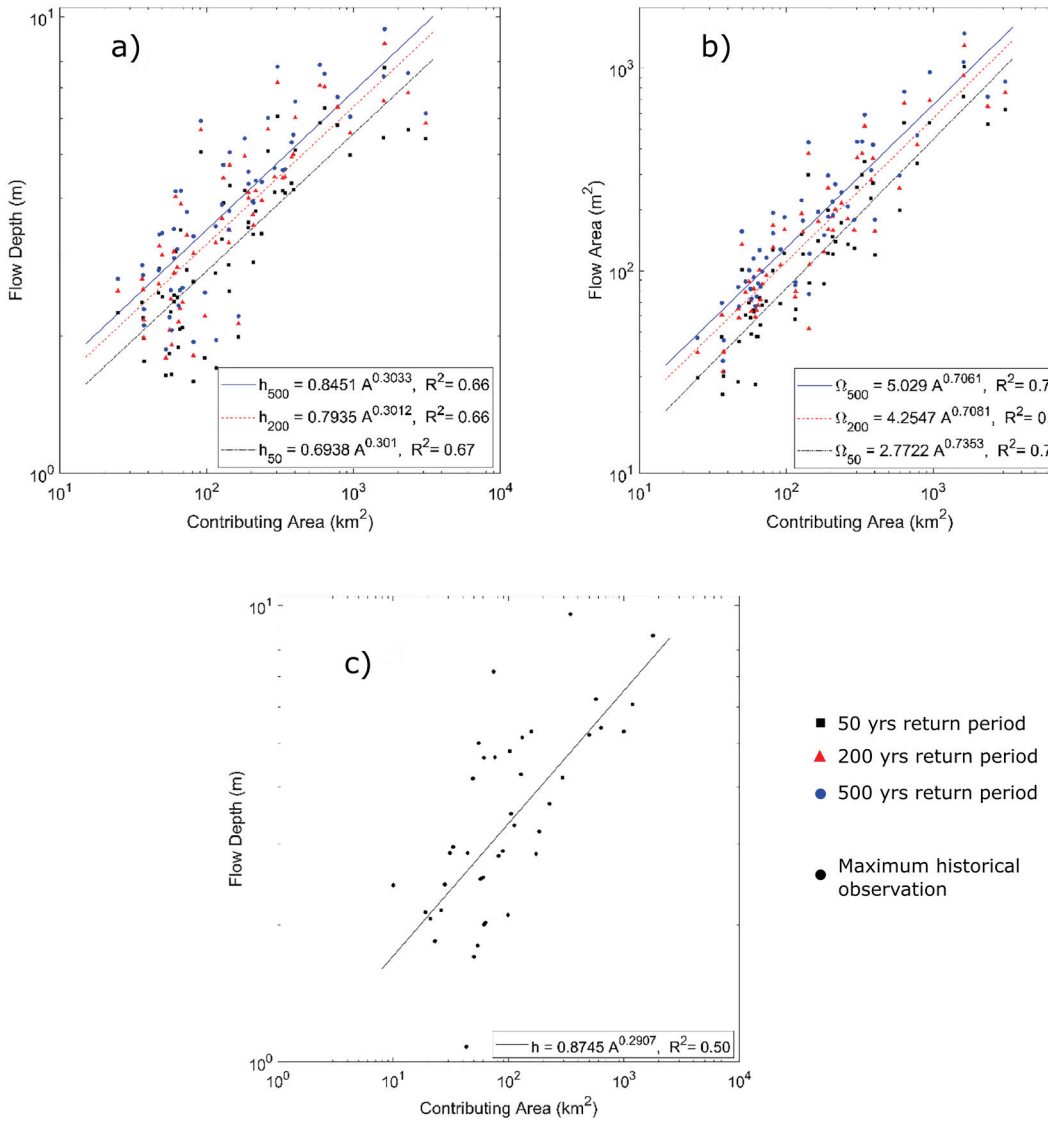

Fig. 2. (a) Flow-depth scaling laws (FD) in Eq. (1) and (b) flow-area scaling laws (FA) in Eq. (2) estimated by log-log regression (colours and linestiles according to return periods) of flow depths and flow areas versus contributed area at 56 cross-sections in Sardinia, obtained through hydraulic modelling for return periods of 50 years (black squares), 200 years (red triangles) and 500 years (blue circles); (c) Flow-depth scaling laws (FD) in Eq. (1) calibrated using maximum historical streamflow observation at 42 gauging stations in Sicily (black circles).

area below h_{rs}, see the filled shape in Fig 1a) calculated through numerical integration equals the flow area Ω_{rs}. The accuracy of the estimated flow depth h_{rs}^{FA} is greatly influenced by the resolution of the DEM utilized for the extraction of the cross-section shape. The choice of the optimal resolution of the DEM to be used in the application of Eq. (3) represents a crucial step of the process. This is because DEM's resolution affect the estimation of flow area associated with a given depth: low resolution DEMs, which are free available, are expected to lead to biased flow area. In this study, we carried out a visual comparison between river cross-sections extracted from DTMs with different resolution: while the river channel geometry was correctly represented using the 1-m and 2-m resolution DTMs (in Sardinia and in Sicily, respectively), 10-m resolution DTMs provided unreliable results (in both cases).

Once the stream network is obtained through the initial terrain analysis, as described at the beginning of this Section, the automatic procedure used to determine the flow depth h_{rs}^{FA} is applied to the selectd river cross-sections extracted from the DEM. To guarantee gradual variations of channel geometry along the river, a reasonable spacing between the cross-sections must be adopted: in our application, a maximum distance of 20 meter between consecutive cross-sections was considered appropriate. In the supplementary materials, the location of considered cross sections for one of the case study basins is depicted as an example (Figure S2).

While flow depths h_{ij}^{FD} and h_{ij}^{FA} assessed through Eqs. (1)–(5) are directly employed in HGM-FD and HGM-FA as a flood descriptor for detecting the flood-prone areas in a river basin of interest, GFIM-FD and GFIM-FA make use of the Geomorphic Flood Index GFI^{FD} (Samela et al., 2017) and a variation of this composite index, hereafter named GFI^{FA}:

$$GFI_{ij}^{FD} = \ln\left(\frac{h_{ij}^{FD}}{H_{ij}}\right) \tag{6}$$

$$GFI_{ij}^{FA} = \ln\left(\frac{h_{ij}^{FA}}{H_{ij}}\right) \tag{7}$$

Both indices GFI_{ij}^{FD} and GFI_{ij}^{FA} are defined through the ratio of two terms: the flow depth h_{ij}^{FD} or h_{ij}^{FA} and the elevation difference H_{ij} between the DEM elevation z_{ij} in the cell (i,j) and DEM elevation z_{rs} in the nearest river cell (r,s) hydrologically connected to (i,j), according to the path

Table 1
Contingency matrix indicating raster cell labelling for performance evaluation.

	Cell within flood-prone area in benchmark map	Cell outside flood-prone area in benchmark map
Cell within flood-prone area in GFIM map	tp	fp
Cell outside flood-prone area in GFIM map	fn	tn

given by the D8 flow algorithm:

$$H_{ij} = z_{ij} - z_{rs} \tag{8}$$

It is worth noticing that the term H_{ij} can also be seen as an indirect measure of the distance between a specified cell and the source of flood hazard, that is the watercourse. Upstream cells located far away from the river centreline are generally characterised by high H_{ij} and low GFI values, while moving closer to the stream, it is expected that H_{ij} decreases and consequently GFI increases according to Eqs. (6) and (7), indicating a greater exposure to flood hazard.

2.2. Calibration of the geomorphic scaling laws

The parameters of Eqs. (1) and (2) have been calibrated by carrying out a regression analysis on data collected in 56 river basins in Sardinia. For each basin outlet, the river cross-section was extracted from a 1-m resolution DTM derived from LiDAR surveys, the upslope contributing area was calculated, and the flood discharges associated with return periods of 50, 200, 500 years were indirectly estimated using regional IDF curves and the rational method formula Kuichling, 1889). Hydraulic modelling with HEC-RAS was then performed to calculate flow depth and flow area values for calibration: for each cross-section, one dimensional steady flow hydraulic simulations were carried out under the hypothesis of uniform flow conditions. Parameters of scaling laws in Eqs. (1) and ((2) with associated return period were obtained by linear regression in log-log space of flow depth or flow area versus contributing area (see Fig. 2a and b).

Under the hypothesis of climatological and hydrological similarities of the two islands (Sicily and Sardinia), it has been here assumed that the parameters calibrated in Sardinia could be applied also in Sicily. This hypothesis of transferability was verified by exploiting gauge data recorded in Sicily and stored in the Italian Institute for Environmental Protection and Research database (http://www.bio.isprambiente.it/annalipdf/). Historical streamflow observations at 42 gauging stations were employed to carry out a linear regression in log-log space of the highest flow depth recorded in each station and the corresponding contributing area value (see Fig. 2c). The constant and the exponent parameters derived from the regression model are very close to the values of the relationships valid for the Sardinian river basins (i.e. for 500 years of return period $a = 0.84$ and $b = 0.30$ in Sardinia, while $a = 0.87$ and $b = 0.29$ in Sicily). Therefore, the hypothesis of parameters transferability was considered acceptable by authors.

2.3. Floodplain delineation

The four approaches for the identification of flood-prone areas described in previous Section were implemented in a Python routine, following the workflow presented by Samela et al. (2018) and Nardi et al. (2019).

HGM-FD and HGM-FA methods make direct use of the two raster grids containing h_{ij}^{FD} and h_{ij}^{FA} flow depth values, which represent the flood descriptors used to define the floodplain extent, respectively. In both methods, cells *(i,j)* where flow depth value h_{ij}^{FD} or h_{ij}^{FA} exceeds or equals the corresponding elevation difference H_{ij} identify areas exposed to flood hazard in the resulting floodplain layer. Conversely, flood-prone areas delineation in the GFIM-FD and GFIM-FA methods require additional steps and relies in a threshold binary classification based on GFI_{ij}^{FD} and GFI_{ij}^{FA} flood descriptors, respectively.

The first step in the GFIM-FD and GFIM-FA methods is thus the setting of an optimal threshold on GFI^{FD} and GFI^{FA} flood descriptors to generate the flood-prone area maps that best reproduce the government agency derived flood hazard map used as a benchmark. To explore the entire range of possible values, both flood descriptors have been rescaled to vary between −1 and 1. The optimal threshold of each index has been calibrated over a limited area of the river basin of interest, namely larger than 2% of the total drainage area as suggested by Samela et al. (2017). Since any choice of threshold defines a unique binary flood-prone area extent, the optimal threshold can be obtained by maximizing specific objective functions that evaluate the degree and matching accuracy of cells labelled as flooded or not with the corresponding cells of the benchmark map. The selected objective functions are thus based on 2 × 2 contingency matrix containing the number of raster cells classified as true positive (tp), false negative (fn), false positive (fp), and true negative (tn), see Table 1.

For identifying the optimal thresholds of the GFI^{FD} and GFI^{FA}, the critical success index (CSI) (Bates and De Roo, 2000; Aronica et al., 2002), the measure-of-fit index (MOF) (Pappenberger et al., 2007), and the true skill statistic (TSS) (Peirce, 1884) have been initially considered and individually used as objective functions to be maximized:

$$CSI = \frac{tp}{tp + fn + fp} \tag{9}$$

$$MOF = \frac{tp - fn}{tp + fn + fp} \tag{10}$$

$$TSS = \frac{tp}{tp + fn} - \frac{fp}{tn + fp} \tag{11}$$

The CSI and the TSS vary between 0 and 1, while the MOF ranges from −1 to 1. For each index, the maximum value is reached when the generated flood map perfectly matches the benchmark, while the minimum indicates that there is no agreement with the reference map.

Since this process requires the availability of an official flood hazard map over a portion of the river basin of interest to calibrate an optimal threshold, it is expected that the GFIM-FD and GFIM-FA are able to provide better mapping performance than the HGM-FD and HGM-FA, which do not apply any binary classification technique.

2.4. Performance assessment

To evaluate the performance of the four considered approaches the CSI described by Eq. (9) was selected together with four metrics provided in the following equations, namely, the true positive rate (TPR), the false positive rate (FPR), the false discovery rate (FDR), and the error bias I:

$$TPR = \frac{tp}{tp + fn} \tag{12}$$

$$FPR = \frac{fp}{fp + tn} \tag{13}$$

$$FDR = \frac{fp}{tp + fp} \tag{14}$$

$$E = \frac{fp}{fn} \tag{15}$$

The TPR, also known as the hit rate, represents the probability of correctly detecting cells subject to flood hazard. It is helpful for quantifying the tendency to underestimate flood-prone areas, but it does not

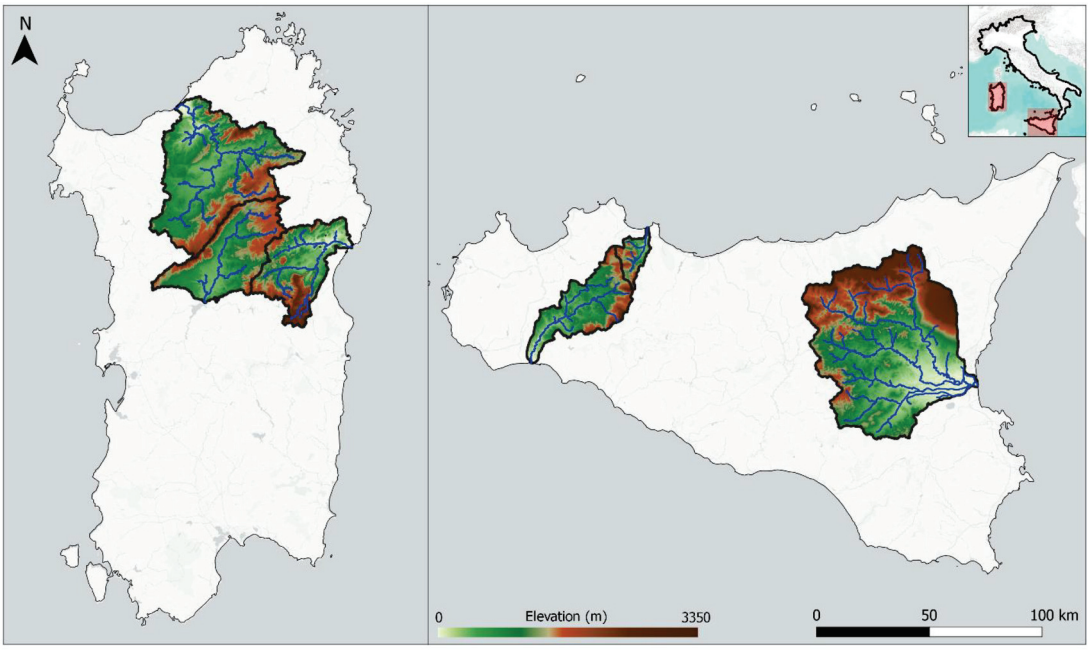

Fig. 3. Geographical location of the investigated area comprising six river basins of Sardinia and Sicily, southern Italy.

Table 2
Case studies main characteristics.

River Basin	Drainage Area [km^2]	Mainstream Length [km]	Mean elevation [m a. s.l.]
Upper Tirso	1305	83	485
Coghinas	2500	115	435
Cedrino	1070	77	485
Simeto	4190	116	530
Belice	960	95	420
Eleuterio	202	30	505

provide any information about overestimation. Conversely, the FPR and the FDR assess this type of deficiency, as they define respectively the probability of incorrectly classifying cells as flooded and the proportion of the overestimation over the total number of instances labelled as positive. These three indices assume values ranging from 0 to 1. The error bias, given by the ratio between false positive and false negative instances, indicates whether the model presents no bias ($E = 1$) or is affected by a general tendency either towards overprediction ($E>1$) or underprediction ($0 \leq E<1$). Overall, the critical success index can be considered as the most informative metric, since it is able to provide a global measure of the mapping performance, in view of the fact that it takes into account both effects of overestimation and underestimation.

Regarding the two methods based on the binary classification (GFIM-FD and GFIM-FA), it is important to remark that the choice of the objective function used to calibrate the optimal threshold for each river basin can significantly affect the resulting flood map. Among the three indices initially selected for calibration, the critical success index (CSI) has been considered the most balanced in penalising overestimation and underestimation, hence the most adequate objective function to be maximized. In fact, the true skill statistic (TSS) tends to favour over-prediction as it does not adequately penalise the false alarm instances through the false positive rate (Pappenberger et al., 2007); this in-efficiency could be handled by selecting a calibration area with balanced binary classes (flooded areas and not-flooded areas). Also, the measure-of-fit (MOF), by additionally penalising underprediction, leads to lower optimal threshold values which are subsequently responsible for a tendency towards overestimation of flooded areas (see Table S1 in the supplementary materials for further details). Given these consider-ations, results for the methods relying on binary classification are referred to the floodplain maps obtained by applying the optimal thresholds derived through the maximization of the critical success index.

3. Study area and data source

The analysis was conducted, as anticipated, in the two largest islands in the Mediterranean Sea, Sicily and Sardinia. Located in southern Italy, the two islands show similar hydrological and climatological features typical of Mediterranean areas. The climate is characterised by a marked seasonality with hot, dry summers and mild, wet winters. Precipitations are mainly concentrated during autumn and winter months with strong interannual variations which are occasionally responsible for arid multi-year periods and droughts. In Sardinia the average annual precipitation is about 650 mm, ranging between 500 mm in flat regions and 1160 mm observed in the mountainous areas (Mascaro et al., 2018). The average annual rainfall in Sicily is about 715 mm, ranging between 400 and 1300 mm from south-eastern to north-eastern regions, respectively (Caracciolo et al., 2018).

The four considered methods were tested on three of the largest river basins in Sardinia, namely Tirso, Coghinas and Cedrino, and three river basins located in Sicily, that are Simeto, Belice and Eleuterio (see Fig. 3), whose main characteristics have been summarised in Table 2. These six catchments were chosen with the purpose of considering a wide range of morphological and hydrological characteristics (e.g., drainage area, stream order, average annual rainfall), as well as including the case of rivers affected by the presence of hydraulic infrastructures.

A simple morphological analysis of the river basins along with the computation of the flood descriptors can be easily performed using the information contained in DEMs. In this work, we utilized freely available DTMs derived from LiDAR surveys with 1-m resolution in Sardinia and 2-m resolution in Sicily, respectively. In addition, 10-m spatial resolution DTMs were employed to investigate how floodplain mapping performance vary with resolution. It is important to remark that 1-m resolution DTMs coverage in Sardinia is only extended to the nearest areas along the major rivers in the island and coastal areas, while the 10-m resolution DTMs are available on the entire regions.

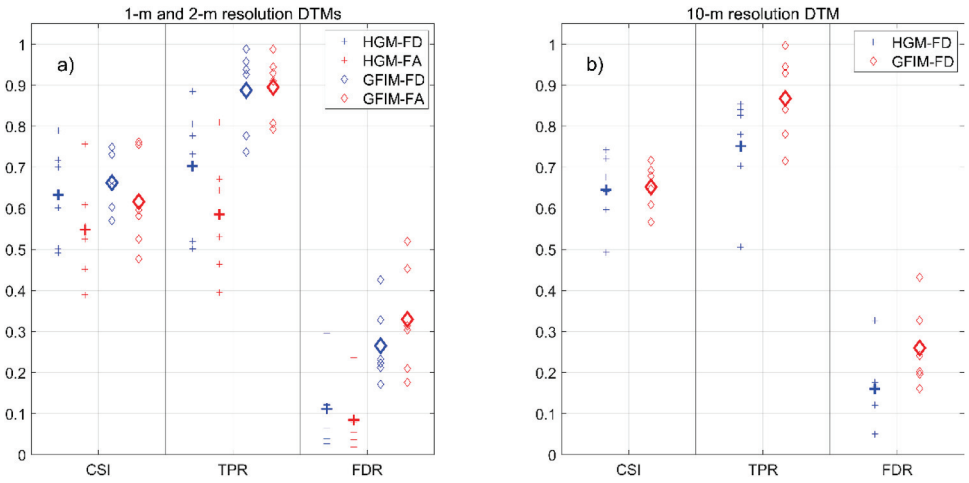

Fig. 4. Critical success index (CSI), true positive rate (TPR), and false discovery rate (FDR) for the four approaches applied over the six river basins: plus (diamond) symbols refer to HGM (GFIM) methods, while blue (red) colours refer to FD (FA) scaling laws adopted; bigger markers display the average metric over all basins for each method and metric. (a) results from 1-m and 2-m resolution DTMs derived from LiDAR surveys; (b) results from the 10-m resolution DTM.

Table 3
Average values of critical success index ($\overline{CSI}$), true positive rate ($\overline{TPR}$), false discovery rate ($\overline{FDR}$), and error bias ($\overline{E}$) over all basins for each method. Basins with best and worst performance in terms of critical success index (CSI) are reported in the right columns. Results from 1-m and 2-m (10-m) resolution DTMs are reported in the upper (bottom) part of the Table.

Input DTM resolution	Method	$\overline{CSI}$	$\overline{TPR}$	$\overline{FDR}$	$\overline{FPR}$	$\overline{E}$	Best performance	Worst performance
1-m & 2-m	HGM-FD	0.6338	0.7035	0.1115	0.0028	0.6	Coghinas, CSI = 0.7895	Alto Tirso, CSI = 0.4916
1-m & 2-m	HGM-FA	0.5481	0.5859	0.0845	0.0017	0.2	Coghinas, CSI = 0.7568	Alto Tirso, CSI = 0.3895
1-m & 2-m	GFIM-FD	0.6626	0.8875	0.2656	0.0120	14.1	Coghinas, CSI = 0.7493	Belice, CSI = 0.5702
1-m & 2-m	GFIM-FA	0.6164	0.8954	0.3295	0.0260	17.7	Belice, CSI = 0.7620	Simeto, CSI = 0.4771
10-m	HGM-FD	0.6452	0.7518	0.1602	0.0013	0.9	Belice, CSI = 0.7423	Simeto, CSI = 0.4926
10-m	GFIM-FD	0.6520	0.8680	0.2602	0.0100	39.3	Simeto, CSI = 0.7173	Belice, CSI = 0.5666

As a benchmark we used the official flood hazard maps developed in the context of the "Piano Stralcio delle Fasce Fluviali" (PSFF) and the "Piano per l'Assetto Idrogeologico" (PAI) by the River Basin Authorities (RBAs) operating in Sardinia and Sicily. According to the European Flood Directive 2007/60/EC, these two documents provide the necessary information to develop guidelines and measures leading to a safer and more sustainable urban development. The PSFF maps available in Sardinia were derived for return periods of 50, 200, and 500 years, while the PAI flood hazard maps available in Sicily are associated with return periods of 50, 100 and 300 years. For the identification of flood-prone areas, the RBAs followed traditional floodplain mapping procedures involving high-precision topographic data collection, hydrologic analysis, and hydraulic modelling.

In this study, the two maps with the highest return periods have been taken as a benchmark to assess the performance of the proposed approaches (namely 500 years for Sardinia and 300 years for Sicily). Again, for sake of clarity, due to the limited availability of 1-m resolution DTMs in Sardinia, performance at this resolution were evaluated considering only the reference flood-prone areas inside the LiDAR data coverage.

4. Results

The four proposed geomorphic approaches were applied to delineate the flood-prone area extents for each river basin in the study area, using high resolution DTMs derived from LiDAR surveys (1-m and 2-m resolution) as the main input. To explore the variability of the mapping performance at a coarser resolution, the HGM-FD and the GFIM-FD have also been implemented making use of 10-m resolution DTMs. This test was not conducted for the HGM-FA and the GFIM-FA, which apply the flow-area scaling laws in Eq. (2), as the river cross-section shape extracted from the 10-m resolution DTMs have been proved inaccurate in representing the channel geometry, especially in complex topography.

After completing the calibration phase, performances of the four considered approaches were evaluated in terms of critical success index (CSI), true positive rate (TPR) and false discovery rate (FDR), see Eqs. (12)–(15) in Section 2.4. Evaluations of such metrics on the 1-m and 2 m resolution DTMs in each of the six selected basins are displayed in Fig. 4a, from where some conclusions can be drawn: (i) hydrogeomorphic methods (HGM-FD and HGM-FA) are affected by higher dispersion of both the critical success index (CSI) and the true positive rate (TPR) compared to the GFIM-FD and GFIM-FA approaches; (ii) GFIM-FD and GFIM-FA approaches performs better in terms of true positive rate (TPR), but at the expense of larger false discovery rate (FDR) with respect to HGM-FD and HGM-FA, suggesting an overestimation tendency of floodplain extension for the former approaches.

For each method and each metric, the average values over the six investigated basins are also plotted in Fig. 4a (with larger symbols) and reported in the upper part of Table 3 (hereafter indicated with overbars as $\overline{CSI}$, $\overline{TPR}$, $\overline{FPR}$, $\overline{FDR}$, and $\overline{E}$). All the implemented approaches provided moderate to high average of critical success index and true positive rate (with $\overline{CSI}$ values ranging from 0.55 to 0.66 and values of $\overline{TPR}$ varying between 0.59 and 0.89) and moderate to low $\overline{FDR}$ values (ranging from 0.33 to 0.08). Below we will draw some considerations on the average performances of the two scaling laws (FD and FA) and the two flood descriptors employed in HGM and GFIM, respectively.

The HGM-FD and GFIM-FD, both employing "flow-depth scaling law" (FD), are characterized by higher critical success index ($\overline{CSI} \approx 0.65$) compared to HGM-FA and GFIM-FA making use of the "flow-area scaling law" (FA) approaches ($\overline{CSI} \approx 0.58$). Similar conclusion applies to the true positive rate ($\overline{TPR} \approx 0.80$ for FD and average

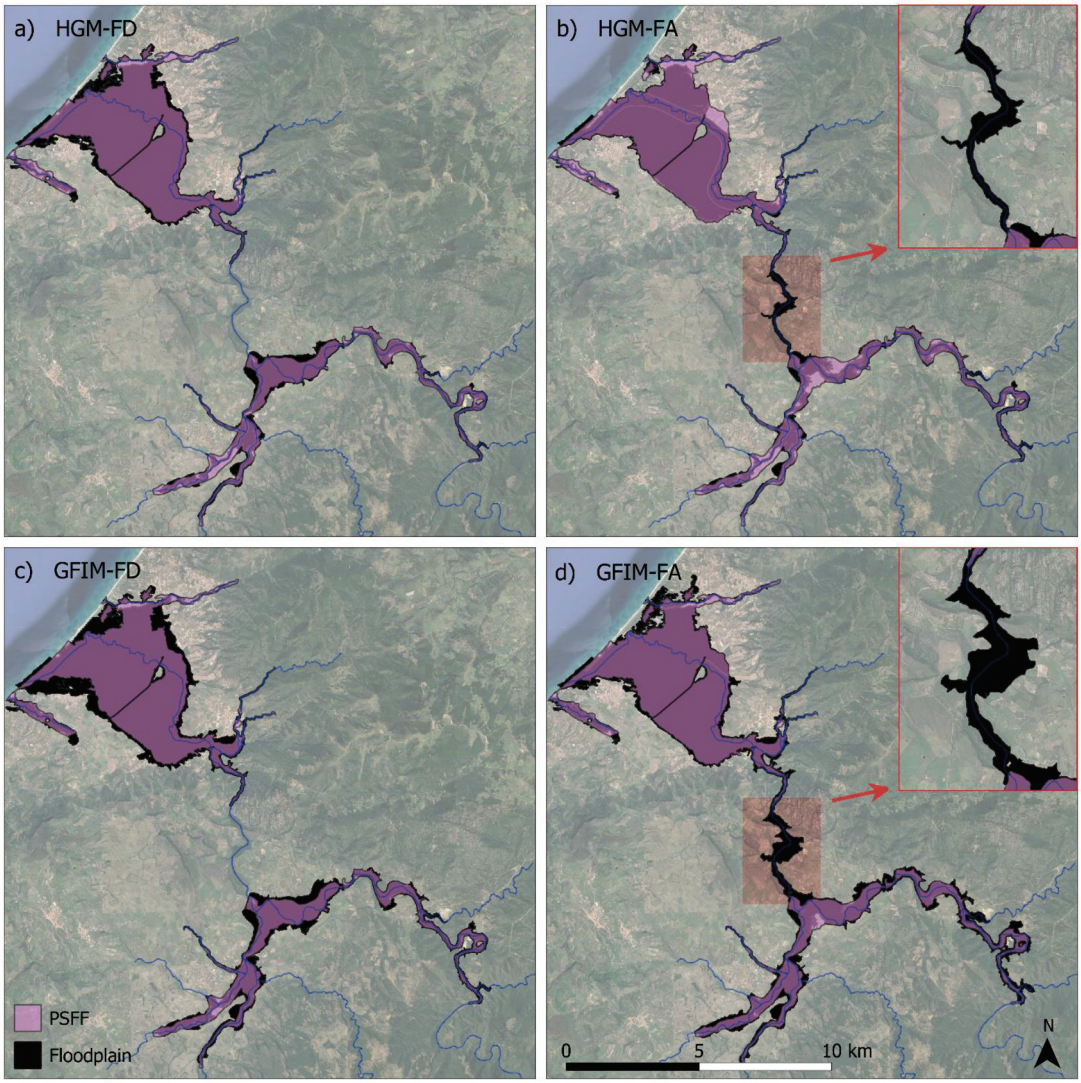

Fig. 5. Official flood hazard identified in the PSFF (depicted in purple) for the Coghinas river basin and flood-prone area extents delineated with the four geomorphic approaches, using as the main input the DTM with 1-m resolution (depicted in black), namely: a) HGM-FD, b) HGM-FA, c) GFIM-FD, d) GFIM-FA. The insets in b) and d) show the Lake Casteldoria being erroneous identified as part of the flooded areas by HGM-FA and GFIM-FA.

$\overline{TPR} \approx$ 0.74 for FA), whilst averages of the false discovery rate and the error bias of the FD-based approaches ($\overline{FDR} \approx$ 0.19, $\overline{E} \approx$ 7.3) are slightly lower compared with FA-based approaches ($\overline{FDR} \approx$ 0.20, $\overline{E} \approx$ 9.0). In five river basins out of six, the method based on FD scaling laws outperformed the others in terms of critical success index: in half of the cases, it was the GFIM-FD, and in one third of the selected catchments the best performance was attributed to the HGM-FD; in the remaining river basin, the GFIM-FA obtained the highest value of CSI (see Table S2 in supplementary materials). Results described above show that the approaches employing FD scaling laws are preferable to FA-based approaches. In fact, parameterization of flow-depth scaling laws in Eq. (1) not only has been proved more efficient by leading to better outcomes in most cases, but it is also easier and faster to be implemented in a GIS environment.

Looking at the relative performances of the two adopted flood descriptors, we can observe from Table 3 that the GFIM-FD and GFIM-FA display greater true positive rate values ($\overline{TPR} \approx$ 0.89) than the HGM-FD and HGM-FA ($\overline{TPR} \approx$ 0.64), but at the same time they exhibit higher false discovery rate ($\overline{FDR} \approx$ 0.30 for GFIM vs $\overline{FDR} \approx$ 0.10 for HGM). This behaviour is explained by the results in error bias values, indicating that both methods based on binary classification overestimate flood-prone areas ($\overline{E} \approx$ 15.9 for GFIM vs $\overline{E} \approx$ 0.4 for HGM). As expected, the HGM-FD and HGM-FA tend to be less performant in terms of critical success index ($\overline{CSI} \approx$ 0.59) than the GFIM-FD and GFIM-FA ($\overline{CSI} \approx$ 0.64) since the optimal thresholds of the two indices are calibrated on limited portions of the study area by taking advantage of benchmark maps derived from hydraulic modelling. Although it allows to achieve better outcomes, the fact that binary classification methods depend on the availability of existing flood hazard maps represents a limitation to their applicability.

Analysing in a deeper detail the performances of the GFIM approaches, we observe that GFIM-FD shows lower average FDR and error bias ($\overline{FDR}$ and $\overline{E}$ equal to 0.27 and 14.4 respectively) than GFIM-FA ($\overline{FDR}$=0.33, $\overline{E}$=17.7), but their average true positive rate TPR values do not significantly differ (both close to 0.89). In other words, the GFIM-FA tends to overestimate flood-prone areas more than the GFIM-FD does, and this is reflected also on the average critical success index, which is in fact higher for the GFIM-FD than the GFIM-FA ($\overline{CSI}$ equal to 0.66 and 0.62 respectively).

Looking in details at performances of the HGM approaches, we observe that HGM-FA presents a slightly lower average FDR than HGM-FD ($\overline{FDR}$ = 0.08 and 0.11 respectively) and the same tendency applies to

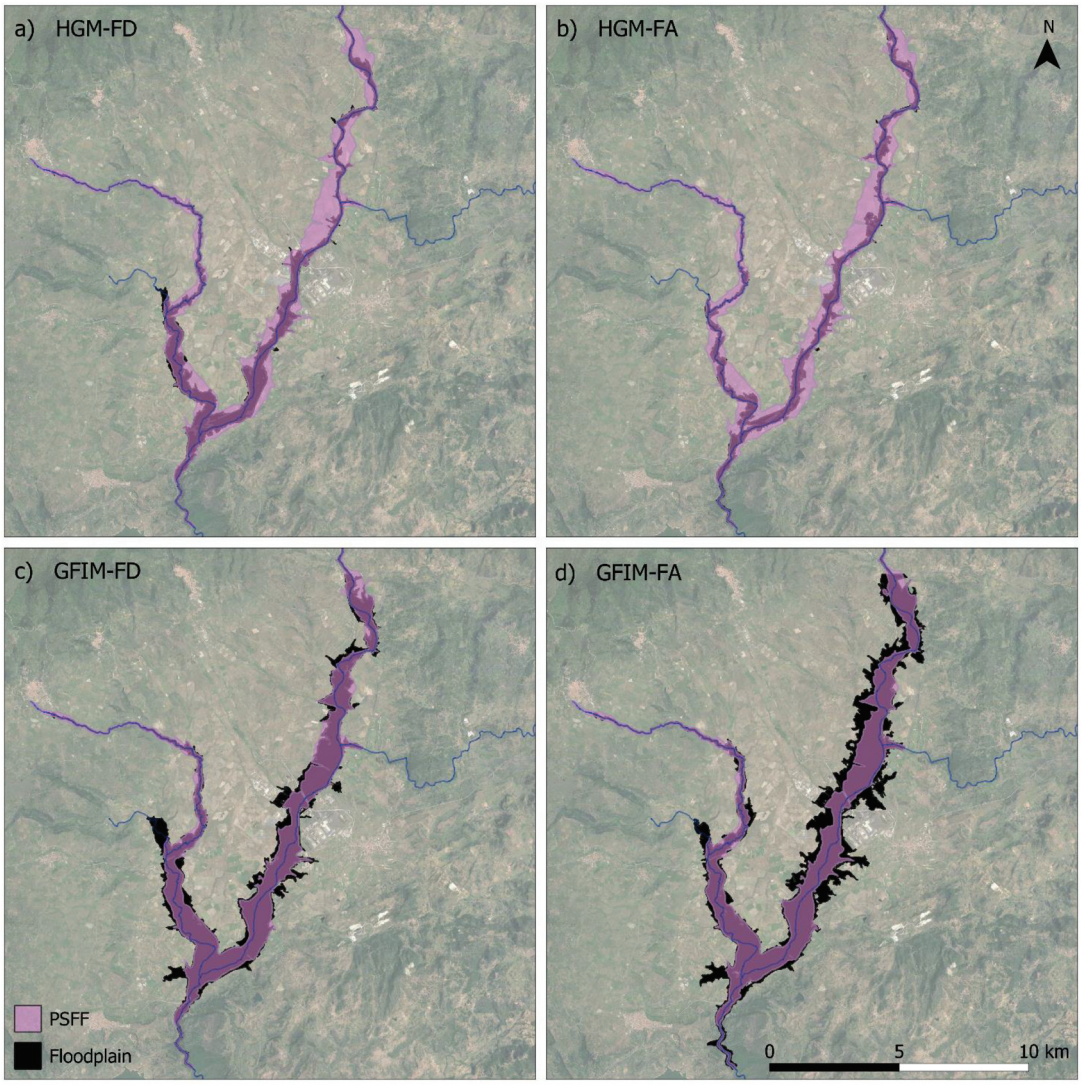

Fig. 6. As Fig. 5 but for the Alto Tirso river basin.

the average error bias ($\overline{E}$ equal to 0.2 and 0.6 respectively). Moreover, the HGM-FD is on average characterized by greater values of true positive rate and critical success index compared to the HGM-FA ($\overline{TPR} =$ 0.70 and $\overline{CSI} =$ 0.63 as opposed to 0.59 and 0.55), revealing that the HGM-FA is the approach that suffers the most from underestimation.

5. Discussion

Although HGM-FA seems to be the least accurate out of the four analysed geomorphic methods in reproducing the flood hazard areas identified in the benchmark maps, it still provides comparable results as its average critical success index is only 10% lower than the highest $\overline{CSI}$ value obtained from the other approaches. The peculiarity of HGM-FA approach consists in the use of the flow-area scaling laws (FA) in Eq. (2), relating cross-sectional flow area to drainage area, which involves the extraction of the stream cross section for the estimation of flow depth values through the FDFA relationship in Eq. (3). This process allows to take greater account of river morphology and channel shape changes. The GFIM-FA is also based on the flow-area scaling laws (FA) in Eq. (2), but the flow depth values provided by the FDFA relationship in Eq. (3) are used to formulate a composite index, the GFI^{FA} in Eq. (7), utilized as a flood descriptor. In this latter case, the floodplain delineation is obtained through a threshold binary classification that slightly enhances the performance, although causing overestimation. The GFIM-FD, taking advantage as well of the binary classification technique, but applying the flow-depth scaling law in Eq. (1), obtained the highest average critical success index among the four compared methods. Nevertheless, the HGM-FD could be considered the most promising in identifying the flood-prone areas since it offers the best compromise between accuracy and computational costs. Using high resolution DEMs as the main input, HGM-FD is the simplest method among the four considered approaches: since the flow depth is obtained with Eq. (1) and directly used as a flood descriptor, this method does not require any extraction of cross-sections along the stream nor the availability of flood hazard maps for threshold calibration purposes (as it is the case of methods applying binary classification).

Examples of floodplain delineation obtained with the four methods along with the flood inundated areas of the benchmark map are depicted in Fig. 5 (best case) and Fig. 6 (worst case) respectively, while maps for the remaining four rivers have been reported in supplementary materials (Figure S3- S6). The visual comparison in Fig. 5 shows that all methods produced reliable flood-prone area extents for the Coghinas river basin. Interestingly, three of the four methods provided their best performance on this catchment, with critical success index ranging between 0.75 and 0.79. In accordance with previous observations, the HGM-FA (Fig. 5b) tends to slightly underestimate floodplain extensions

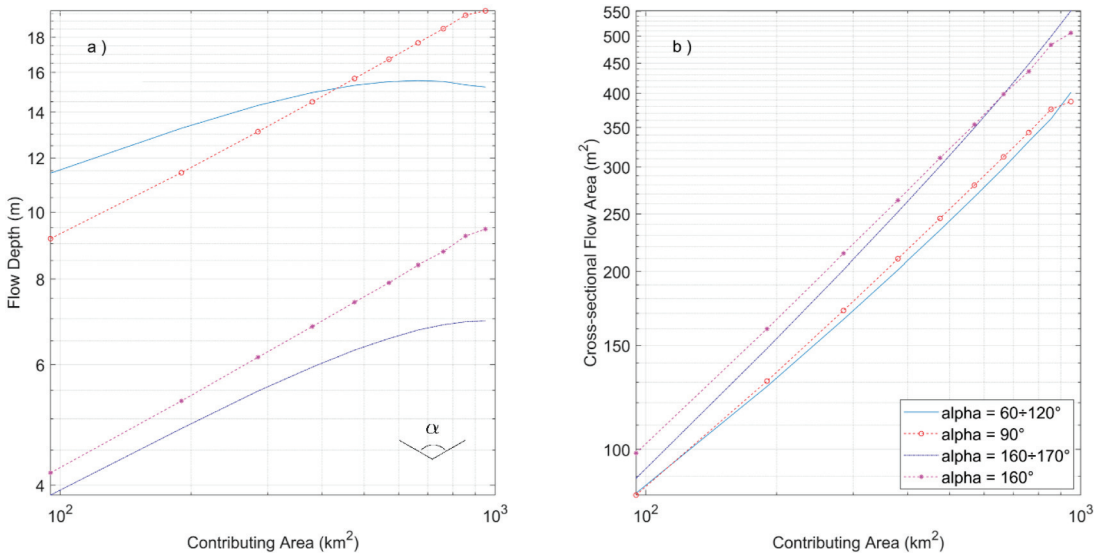

Fig. 7. Relationships between flow depth and contributing area (a) and flow area and contributing area (b) referred to a synthetic case conducted on a rectangular river basin with discharge increasing linearly with drainage area and river channel geometry approximated through triangular cross-sections. Two different configurations of stream geometry were tested: i) constant riverbanks slope (alpha=90° and alpha=160°); ii) progressive decrease in riverbanks slope moving from upstream to downstream cross-sections (alpha=60÷120° and alpha=160÷170°).

(E<1), while the GFIM-FD (Fig. 5c) and GFIM-FA (Fig. 5d) are affected by a tendency towards overestimation (E>1); the HGM-FD presents no bias ($E = 1$). Although stream morphology is taken into greater consideration in the methods applying flow-area scaling laws in Eq. (2) rather than those based on FD scaling laws in Eq. (1), a paradigmatic case is offered by the Lake Casteldoria, originated by the Casteldoria dam, erroneously identified as exposed to flood hazard by both methods HGM-FA and GFIM-FA (see insets in Fig. 5b and d). This drawback is due to the very steep flow depth-flow area relationship in Eq. (3) corresponding to the narrow shape of the channel at the first cross-section downstream the dam: as a result, the high flow depth corresponding to the estimated flow area exceeded the difference in elevation between the upstream cells included into the reservoir and the stream cell belonging to the cross-section, causing the false positive instances. In the HGM-FD and GFIM-FD this circumstance does not occur as the flow depth is exclusively dependent on the drainage area, therefore any effect induced by changes in channel geometry is completely neglected. A further investigation of this specific case also revealed a significant underestimation of the flow depth provided by FD scaling laws in Eq. (1), but since this happens in a deep canyon even a large error in flow depth estimation leads to the same mapping outcome by FD-based approaches. Conversely, the erroneous mapping resulting from the FA based approaches seems to be mainly related to an overestimation of the flow area, due to the fact that the flow-area scaling laws in Eq. (2) were mainly calibrated on wide cross-sections and gentle riverbed profiles.

Fig. 6 displays a sample of the flood-prone areas identified in the Alto Tirso river basin, where the HGM-FD and HGM-FA exhibited their poorest performance, with critical success index of 0.49 and 0.39 respectively. Both methods, especially the HGM-FA, tend to strongly underestimate flooded areas (E<1), whilst the two approaches based on binary classification suffer once again from overestimation (E>1).

Regarding the sensitivity of the approaches to varying input resolution, the outcomes of the HGM-FD and GFIM-FD tested with the 10-m resolution DTMs do not significantly differ from the results obtained by the 1-m and 2-m resolution DTMs: in terms of average success index the percentage difference is below 2%, with the HGM-FD performing slightly better at coarser resolution in opposition to the GFIM-FD, which is marginally less performant; also, the metrics dispersion are extremely similar (see Fig. 4b). In four river basins out of six the GFIM-FD produced the highest value of CSI, nevertheless the average critical success index for both methods is equal to 0.65. The general behaviour identified at finer resolution is maintained: the HGM-FD tends to underestimate flooded areas (E<1), while the GFIM-FD is still characterised by overestimation bias (E>1). Overall, in this investigation the two methods implementing the flow-depth scaling laws did not show significant sensitivity to the DTMs resolution change from 1-m and 2-m to 10-m.

At the same time, it is worth mentioning that for FA methods the analyses were not even possible with the 10-m resolution DTMs because the cross-sectional area estimation turns out to be unreliable. Only high resolution DEM, as the ones provided by LiDAR, allow to correctly estimate the cross-sectional area and take into account the presence of levees, roads and bridges embankments, and in general any artificial or natural changes in elevation that are impossible to detect with such accuracy at coarser resolutions. Considering that FA approach involves terrain analysis and utilizes as a main input the topographic information contained in DTMs, for its application it would be reasonable to utilize the highest resolution terrain data available.

6. Conclusions

The present study investigated the floodplain mapping performance of four geomorphic approaches based on the coupling of two flood descriptors (HGM and GFIM) and two simple power laws (flow-depth (FD) and flow-area (FA) scaling laws) relating flow depth and cross-sectional flow area to upstream contributing area. Six river basins located in southern Italy were selected as a case study and their flood-prone areas were estimated with the four approaches using high resolution DEMs as the main input, and finally compared with official flood hazard benchmark maps derived from hydraulic modelling.

Overall, the implemented methods provided average critical success index varying between 0.55 and 0.66, average true positive rate ranging from 0.59 to 0.89, and average false discovery rate ranging between 0.08 and 0.33. The GFIM-FD and GFIM-FA, based on the threshold binary classification of the GFI to delineate floodplain extents, displayed a tendency towards overestimation, whilst methods directly employing flood depth as flood descriptor suffer from underestimation, especially the HGM-FA. The two methods employing the relationship between flow depth and contributing area (flow-depth scaling laws, FD, Eq. (1)) performed better than the two relating flow area to drainage area (flow-area scaling laws, FA, Eq. (2)), despite not being able to take as much into

consideration the stream morphology. In fact, the highest average critical success index was obtained by GFIM-FD, immediately followed by the HGM-FD, confirming flow depth as a valid flood descriptor to be used in geomorphic approaches. It is important to underline that the methodologies proposed in this work, being based on simple power laws and taking as the main input the information contained in DTMs, are not expected to reproduce exactly the floodplain maps obtained through conventional procedures involving hydrologic and hydraulic modelling. However, they may represent useful tools for approximately delineating flood-prone areas in ungauged basins or in data-scarce regions where standard flood hazard maps are unavailable.

With the increasing availability of high-resolution topographic data, further investigations at regional scale should be carried out to better explore the potentialities of these geomorphic methods, incorporating these DTM based approaches into machine learning workflows and also to test the transferability of the scaling laws parameters.

CRediT authorship contribution statement

Claudia Deiana: Methodology, Software, Data curation, Writing – original draft. **Roberto Deidda:** Visualization, Investigation, Writing – review & editing, Funding acquisition. **Francesco Viola:** Methodology, Visualization, Investigation, Writing – review & editing.

Declaration of Competing Interest

The authors declare the following financial interests/personal relationships which may be considered as potential competing interests:

Roberto Deidda reports financial support was provided by European Union.

Acknowledgments

The Authors acknowledge and thank the two reviewer, Prof. Salvatore Manfreda and the anonymous one, for their meticulous work and the precious suggestions.

This study was carried out within the RETURN Extended Partnership and received funding from the European Union Next-Generation EU (National Recovery and Resilience Plan – NRRP, Mission 4, Component 2, Investment 1.3 – D.D. 1243 2/8/2022, PE0000005).

Supplementary materials

Supplementary material associated with this article can be found, in the online version, at doi:10.1016/j.advwatres.2023.104493.

Appendix

Regarding the feasibility and performances of methods based on flow-area scaling laws (FA) compared to flow-depth scaling laws (FD), on an empirical basis we initially supposed that the former could potentially have a greater capability of approximately representing what occurs during critical flood events. In fact, while the flow area is expected to tendentially increase moving from upstream to downstream cross-sections of the same river, hence as the drainage area increases, the behaviour of the flow depth is subject to greater uncertainty, especially when the bank-full stage is exceeded. We formulated this hypothesis on the basis of a synthetic case conducted on a rectangular river basin with discharge increasing linearly with contributing area. Hydraulic simulations executed with HEC-RAS in one dimensional steady flow under uniform conditions, allowed to estimate flow depth and flow area values at the river cross-sections. The stream channel geometry has been approximated through a triangular shape and two different configurations were tested: the former assumed constant riverbanks slope for all the cross-sections along the stream; the latter considered a progressive decrease in riverbanks slope moving from upstream to downstream cross-sections, trying to mimic to the natural downstream changes in channel geometry. While in the first configuration the flow depth increases downstream with increasing contributing area, in the second case it can be observed that after an initial increase, the water depth tends to remain constant or slightly decrease (see Fig. 7a). Instead, the flow area shows an increasing tendency in both configurations (see Fig. 7b), which led to the assumptions explained above. In addition to these empirically based considerations, the fact that flow area has not been employed before as a proxy of a flood descriptor in automatic flood-prone area detection techniques, has contributed to arouse great interest in investigating the potentialities of Eq. (3) for this scope.

References

Annis, A., Karpack, M., Morrison, R.R., Nardi, F., 2022. On the influence of river Basin morphology and climate on hydrogeomorphic floodplain delineations. Adv. Water Res. 159, 104078 https://doi.org/10.1016/j.advwatres.2021.104078.

Aronica, G., Bates, P.D., Horritt, M.S., 2002. Assessing the uncertainty in distributed model predictions using observed binary pattern information within GLUE. Hydrol. Processes 16, 2001–2016. https://doi.org/10.1002/hyp.398.

Bates, P.D., De Roo, A.P.J., 2000. A simple raster-based model for flood inundation simulation. J. Hydrol. 236, 54–77. https://doi.org/10.1016/S0022-1694(00)00278-X.

Bhowmik, N.G., 1984. Hydraulic geometry of floodplains. J. Hydrol. 68, 369–401. https://doi.org/10.1016/0022-1694(84)90221-X. Global Water: Science and Engineering The Ven Te Chow Memorial Volume.

Caracciolo, D., Francipane, A., Viola, F., Noto, L.V., Deidda, R., 2018. Performances of GPM satellite precipitation over the two major Mediterranean islands. Atmos. Res. 213, 309–322. https://doi.org/10.1016/j.atmosres.2018.06.010.

CRED, Centre for Research on the Epidemiology of Disaster, 2020. Human Cost of Disasters (2000-2019). UCLouvain, Brussels, Belgium. https://www.emdat.be/cred-crunch-61-human-cost-disasters-2000-2019-0).

Degiorgis, M., Gnecco, G., Gorni, S., Roth, G., Sanguineti, M., Taramasso, A.C., 2012. Classifiers for the detection of flood-prone areas using remote sensed elevation data. J. Hydrol. 470–471, 302–315. https://doi.org/10.1016/j.jhydrol.2012.09.006.

Deidda, R., Hellies, M., Langousis, A., 2021. A critical analysis of the shortcomings in spatial frequency analysis of rainfall extremes based on homogeneous regions and a comparison with a hierarchical boundaryless approach. Stoch. Environ. Res. Risk Assess. 35 (12), 2605–2628. https://doi.org/10.1007/s00477-021-02008-x.

Forestieri, A., Arnone, E., Blenkinsop, S., Candela, A., Fowler, H., Noto, L.V., 2018. The impact of climate change on extreme precipitation in Sicily, Italy. Hydrol. Processes 32, 332–348. https://doi.org/10.1002/hyp.11421.

Fowler, H.J., Ali, H., Allan, R.P., Ban, N., Barbero, R., Berg, P., Blenkinsop, S., Cabi, N.S., Chan, S., Dale, M., Dunn, R.J.H., Ekström, M., Evans, J.P., Fosser, G., Golding, B., Guerreiro, S.B., Hegerl, G.C., Kahraman, A., Kendon, E.J., Lenderink, G., Lewis, E., Li, X., O'Gorman, P.A., Orr, H.G., Peat, K.L., Prein, A.F., Pritchard, D., Schär, C., Sharma, A., Stott, P.A., Villalobos-Herrera, R., Villarini, G., Wasko, C., Wehner, M.F., Westra, S., Whitford, A., 2021. Towards advancing scientific knowledge of climate change impacts on short-duration rainfall extremes. Philos. Trans. R. Soc. A 379, 20190542. https://doi.org/10.1098/rsta.2019.0542.

Jasiewicz, J., Metz, M., 2011. A new GRASS GIS toolkit for Hortonian analysis of drainage networks. Comput. Geosci. 37, 1162–1173. https://doi.org/10.1016/j.cageo.2011.03.003.

Kuichling, E., 1889. The Relation between the Rainfall and the Discharge of Sewers in Populous Districts. Trans. Am. Soc. Civil Eng. 20 (1), 1–56.

Lehmkuhl, F., Schüttrumpf, H., Schwarzbauer, J., Brüll, C., Dietze, M., Letmathe, P., Völker, C., Hollert, H., 2022. Assessment of the 2021 summer flood in Central Europe. Environ. Sci. 34 (1), 107. https://doi.org/10.1186/s12302-022-00685-1. Europeart. no.

Leopold, L.B., Maddock, T., 1953. The hydraulic geometry of stream channels and some physiographic implications (USGS Numbered Series No. 252). The Hydraulic Geometry of Stream Channels and Some Physiographic Implications. Professional Paper. U.S. Government Printing Office, Washington, D.C. https://doi.org/10.3133/pp252.

Manfreda, S., Di Leo, M., Sole, A., 2011. Detection of flood-prone areas using digital elevation models. J. Hydrol. Eng. 16, 781–790. https://doi.org/10.1061/(ASCE)HE.1943-5584.0000367.

Manfreda, S., Nardi, F., Samela, C., Grimaldi, S., Taramasso, A.C., Roth, G., Sole, A., 2014. Investigation on the use of geomorphic approaches for the delineation of flood prone areas. J. Hydrol. 517, 863–876. https://doi.org/10.1016/j.jhydrol.2014.06.009.

Mascaro, G., Viola, F., Deidda, R., 2018. Evaluation of precipitation from EURO-CORDEX regional climate simulations in a small-scale mediterranean site. J. Geophys. Res. Atmos. 123, 1604–1625. https://doi.org/10.1002/2017JD027463.

Nardi, F., Annis, A., Baldassarre, G.D., Vivoni, E.R., Grimaldi, S., 2019. GFPLAIN250m, a global high-resolution dataset of earth's floodplains. Sci. Data 6. https://doi.org/10.1038/sdata.2018.309.

Nardi, F., Biscarini, C., Di Francesco, S., Manciola, P., Ubertini, L., 2013. Comparing a large-scale DEM-based floodplain delineation algorithm with standard flood maps: the Tiber River basin case study. Irrig. Drain. 62, 11–19. https://doi.org/10.1002/ird.1818.

Nardi, F., Vivoni, E.R., Grimaldi, S., 2006. Investigating a floodplain scaling relation using a hydrogeomorphic delineation method. Water Resour. Res. 42 https://doi.org/10.1029/2005WR004155.

Nobre, A.D., Cuartas, L.A., Momo, M.R., Severo, D.L., Pinheiro, A., Nobre, C.A., 2016. HAND contour: a new proxy predictor of inundation extent. Hydrol. Processes 30, 320–333. https://doi.org/10.1002/hyp.10581.

O'Callaghan, J.F., Mark, D.M., 1984. The extraction of drainage networks from digital elevation data. Comput. Vis. Graph. Image Process. 28, 323–344. https://doi.org/10.1016/S0734-189X(84)80011-0.

Pappenberger, F., Frodsham, K., Beven, K., Romanowicz, R., Matgen, P., 2007. Fuzzy set approach to calibrating distributed flood inundation models using remote sensing observations. Hydrol. Earth Syst. Sci. 11, 739–752. https://doi.org/10.5194/hess-11-739-2007.

Passalacqua, P., Trung, T.D., Foufoula-Georgiou, E., Sapiro, G., Dietrich, W.E., 2010. A geometric framework for channel network extraction from lidar: nonlinear diffusion and geodesic paths. J. Geophys. Res. Earth Surf. 115 https://doi.org/10.1029/2009JF001254.

Peirce, C.S., 1884. The numerical measure of the success of predictions. Science 4, 453–454. https://doi.org/10.1126/science.ns-4.93.453-a.

Rennó, C.D., Nobre, A.D., Cuartas, L.A., Soares, J.V., Hodnett, M.G., Tomasella, J., Waterloo, M.J., 2008. HAND, a new terrain descriptor using SRTM-DEM: mapping terra-firme rainforest environments in Amazonia. Remote Sens. Environ. 112, 3469–3481. https://doi.org/10.1016/j.rse.2008.03.018.

Rodriguez-Iturbe, I., 1993. The geomorphological unit hydrograph. Channel Netw. hydrol. 43–68.

Rodríguez-Iturbe, I., Devoto, G., Valdés, J.B., 1979. Discharge response analysis and hydrologic similarity: the interrelation between the geomorphologic IUH and the storm characteristics. Water Resour. Res. 15, 1435–1444. https://doi.org/10.1029/WR015i006p01435.

Samela, C., Albano, R., Sole, A., Manfreda, S., 2018. A GIS tool for cost-effective delineation of flood-prone areas. Comput. Environ. Urban Syst. 70, 43–52. https://doi.org/10.1016/j.compenvurbsys.2018.01.013.

Samela, C., Troy, T.J., Manfreda, S., 2017. Geomorphic classifiers for flood-prone areas delineation for data-scarce environments. Adv. Water Res. 102, 13–28. https://doi.org/10.1016/j.advwatres.2017.01.007.

Tavares da Costa, R., Zanardo, S., Bagli, S., Hilberts, A.G.J., Manfreda, S., Samela, C., Castellarin, A., 2020. Predictive modeling of envelope flood extents using geomorphic and climatic-hydrologic catchment characteristics. Water Resour. Res. 56, e2019WR026453 https://doi.org/10.1029/2019WR026453.

Zheng, X., Maidment, D.R., Tarboton, D.G., Liu, Y.Y., Passalacqua, P., 2018. GeoFlood: large-scale flood inundation mapping based on high-resolution terrain analysis. Water Resour. Res. 54 (12), 10,013–10,033. https://doi.org/10.1029/2018WR023457.